OPEN ACCESS Freely available online

PLOS ONE

Slip Effects on Mixed Convective Peristaltic Transport of Copper-Water Nanofluid in an Inclined Channel

Fahad Munir Abbasi[1]*, Tasawar Hayat[1,2], Bashir Ahmad[2], Guo-Qian Chen[2,3]

1 Department of Mathematics, Quaid-I-Azam University, Islamabad, Pakistan, **2** Nonlinear Analysis and Applied Mathematics (NAAM) Research Group, Faculty of Science, King Abdulaziz University, Jeddah, Saudi Arabia, **3** College of Engineering, Peking University, Beijing, China

Abstract

Peristaltic transport of copper-water nanofluid in an inclined channel is reported in the presence of mixed convection. Both velocity and thermal slip conditions are considered. Mathematical modelling has been carried out using the long wavelength and low Reynolds number approximations. Resulting coupled system of equations is solved numerically. Quantities of interest are analyzed through graphs. Numerical values of heat transfer rate at the wall for different parameters are obtained and examined. Results showed that addition of copper nanoparticles reduces the pressure gradient, axial velocity at the center of channel, trapping and temperature. Velocity slip parameter has a decreasing effect on the velocity near the center of channel. Temperature of nanofluid increases with increase in the Grashoff number and channel inclination angle. It is further concluded that the heat transfer rate at the wall increases considerably in the presence of copper nanoparticles.

Citation: Abbasi FM, Hayat T, Ahmad B, Chen G-Q (2014) Slip Effects on Mixed Convective Peristaltic Transport of Copper-Water Nanofluid in an Inclined Channel. PLoS ONE 9(8): e105440. doi:10.1371/journal.pone.0105440

Editor: Victor M. Ugaz, Texas A&M University, United States of America

Received February 15, 2014; **Accepted** June 30, 2014; **Published** August 29, 2014

Funding: This paper was funded by the Deanship of Scientific Research (DSR), King Abdulaziz University, Jeddah, under grant no. 9-130/1434 HiCi. The authors, therefore, acknowledge with thanks DSR technical and financial support. The funders had no role in study design, data collection and analysis, decision to publish, or preparation of the manuscript.

Competing Interests: The authors have declared that no competing interests exist.

* Email: abbasisarkar@gmail.com

Introduction

Mixed convective flows have received numerous attention from the researchers the world over due to their wide industrial and engineering applications. Convection is seen in the ocean currents, sea-wind formation, rising of plume of hot air from fire, formation of micro-structures during the cooling of molten metals, solar ponds and in fluid flows around heat dissipation fins. Convection in channels plays a vital role in heat exchangers, removal of nuclear waste and in modern cooling/heating systems. ''Nanofluids'' refer to heat transfer liquids with enhanced heat transfer capability. Such materials are obtained by suspending nanoparticles in traditional heat transfer liquids e.g. water, ethylene glycol and engine oil. A number of experimental studies elaborate that the convective heat transfer in nanofluids is considerably higher than that of the base fluids. Enhanced heat transfer in nanofluids has enabled there use in several electrical and engineering applications. This gives rise to a new branch of mechanics named nanofluid mechanics. The wide utility of nanofluids is the reason for growing interest in nanofluid mechanics by the researchers of modern era. The term nanofluid was introduced by Choi [1] in his effort to enhance the thermal conductivity of the fluids. Buongiorno [2] proposed that thermophoresis and Brownian motion are significant in the dynamics of nanofluids. Some studies using the Buongiorno's model of nanofluids can be seen through refs. [3–5]. Expressions for the effective density and viscosity of the nanofluids were computed by Xuan and Li [6]. Brinkman's [7] model for the effective viscosity of the two phase flow was found to be in good agreement with the experimental results (Xuan and Li. [8]). Tiwari and Das [9] proposed a model for the analysis of nanofluids employing the results of Xuan and Li [6] and Brinkman [7]. Model of Tiwari and Das [9] was used by many researchers for the analysis of nanofluid dynamics and was found in good agreement with the experimental data (see [10–13]).

Peristalsis is a well-known mechanism for fluid transport in physiology. In this mechanism sinusoidal waves travel on the walls of tube like organs of human beings propelling the fluid contained within the tube in the direction of their propagation. In physiology the principle of peristalsis is seen in the transport of food through oesophagus, movement of chyme in intestines, urine transport from kidneys to the bladder, bile transport in bile duct, transport of spermatozoa, vasomotion of blood vessels and many others. Peristalsis has proven very useful in fluid transport over short distance preventing the fluid from being contaminated. Subject to its utility, such mechanism has been adopted by the engineers in designing several industrial appliances including roller and finger pumps and peristaltic pumps in heart lung and dialysis machines. Latest hose pumps of several kinds operate through the principle of peristalsis. Peristaltic type flow is readily being used in the nuclear industry for the transport of corrosive fluids. Subject to such wide occurrence of peristalsis in physiology and industry many theoretical investigations are carried out in different flow configuration [14–22]. It is now well admitted fact that all the tubular organs facilitating fluid flow in human body are internally lubricated with mucus and secretion layers. These layers in turn prevent the fluid from sticking to the walls. In such cases the no-slip condition between the fluid and solid boundary is not valid. With such motivation some authors investigated the peristaltic transport of traditional fluids with slip effects [23–25].

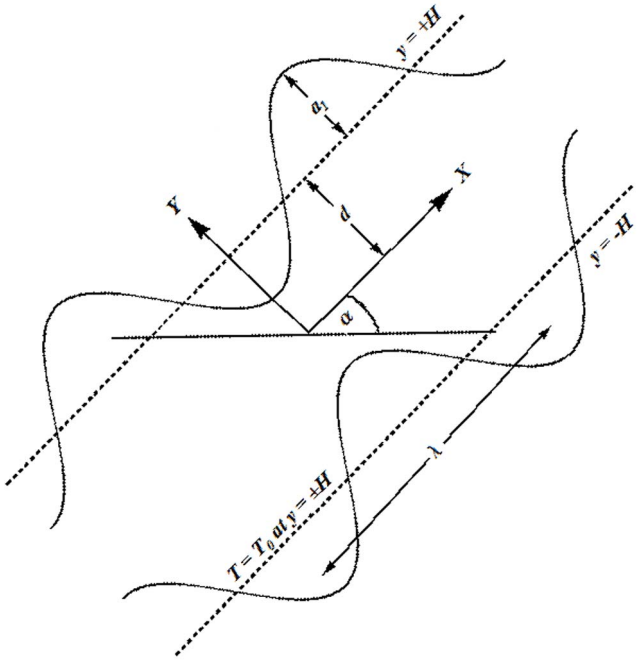

Figure 1. Geometry of the problem.
doi:10.1371/journal.pone.0105440.g001

It is noticed from existing information on the topic that not much has been said yet about the peristaltic motion of nanofluids. Few recent investigations constructed such flow models (see [26–27]). In these attempts, the Buongiorno's model of nanomaterial has been employed. However there is not a single attempt which can address the peristaltic transport of nanofluid employing Tiwari and Das [9] model. Intention in present communication is to prepare such fluid model describing peristalsis. Hence we consider here the copper-water nanofluid to discuss the peristaltic flow in a symmetric channel with slip conditions. The channel walls satisfy the velocity and thermal slip conditions. Inclined channel filled with an incompressible fluid is considered. Relevant modeling is presented. Computations for the governing problems are made numerically. Plots for different flow quantities of interest are displayed and analyzed.

Formulation and Solution

Consider the peristaltic flow of copper-water nanofluid in a symmetric channel of width $2d$. The channel is inclined at an angle α to the horizontal. Moreover the channel walls are maintained at constant temperature T_0. Cartesian coordinates are chosen in such a way that the $\overline{X}$-axis lies along the length of the channel whereas $\overline{Y}$ -axis is normal to $\overline{X}$ -axis. Waves of wavelength λ and amplitude a_1 travel on the channel walls with constant speed c. These waves are responsible for flow generation in the channel. Schematic diagram of the problem is given in Fig. 1.

Wave geometry is of the form

$$\pm\overline{H}(\overline{X},\overline{t}) = \pm d \pm a_1 \cos\left(\frac{2\pi}{\lambda}(\overline{X}-c\overline{t})\right), \qquad (1)$$

where $+\overline{H}$ and $-\overline{H}$ denote the upper and lower walls respectively. Velocity profile for such a flow is $\mathbf{V} = [\overline{U}(\overline{X},\overline{Y},\overline{t}), \overline{V}(\overline{X},\overline{Y},\overline{t}), \overline{0}]$. The two-dimensional continuity equation for an incompressible flow can be written as follows:

Table 1. Nomenclature.

Nomenclature			
$\overline{H}$ $(\overline{X},t)$	Peristaltic wall	d	Half channel width
a_1	Amplitude of peristaltic wave	λ	Wavelength of peristaltic wave
$\overline{U}$	$\overline{X}$-component of velocity	$\overline{V}$	$\overline{Y}$-component of velocity
$\overline{P}$	Pressure	ρ_{nf}	Density of nanofluid
μ_{eff}	Effective viscosity	g	Acceleration due to gravity
β_{nf}	Thermal expansion coefficient of nanofluid	α	Channel inclination angle
T	Temperature	T_0	Temperature of the walls
C_{nf}	Specific heat of nanofluid	K_{eff}	Effective thermal conductivity
Φ	Dimensional heat source/sink parameter	μ_f	Viscosity of base fluid
ρ_f	Density of base fluid	ρ_p	Density of nanoparticles
C_f	Specific heat of base fluid	C_P	Specific heat of nanoparticles
β_f	Thermal expansion coefficient of base fluid	φ	Nanoparticles volume fraction
β_p	Thermal expansion coefficient of nanoparticle	K_f	Thermal conductivity of base fluid
K_p	Thermal conductivity of nanoparticles	E	Eckert number
Re	Reynolds number	Pr	Prandtl number
Gr	Grashoff number	Br	Brinkman number
ψ	Stream function	β	Dimensionless velocity slip parameter
F	Dimensionless volume flow rate in wave frame	γ	Dimensionless thermal slip parameter
η	Dimensionless volume flow rate in fixed frame	Δp_λ	Pressure rise per wavelength

doi:10.1371/journal.pone.0105440.t001

Table 2. Numerical values of the thermophysical properties.

Property	Basefluid/water	Nanoparticles/copper (Cu)
Density (kg/m^3)	997.1	8933
Thermal conductivity (W/mK)	0.613	400
Specific heat (J/kgK)	4179	385
Thermal expansion coefficient (1/K)$\times 10^{-6}$	210	16.65

doi:10.1371/journal.pone.0105440.t002

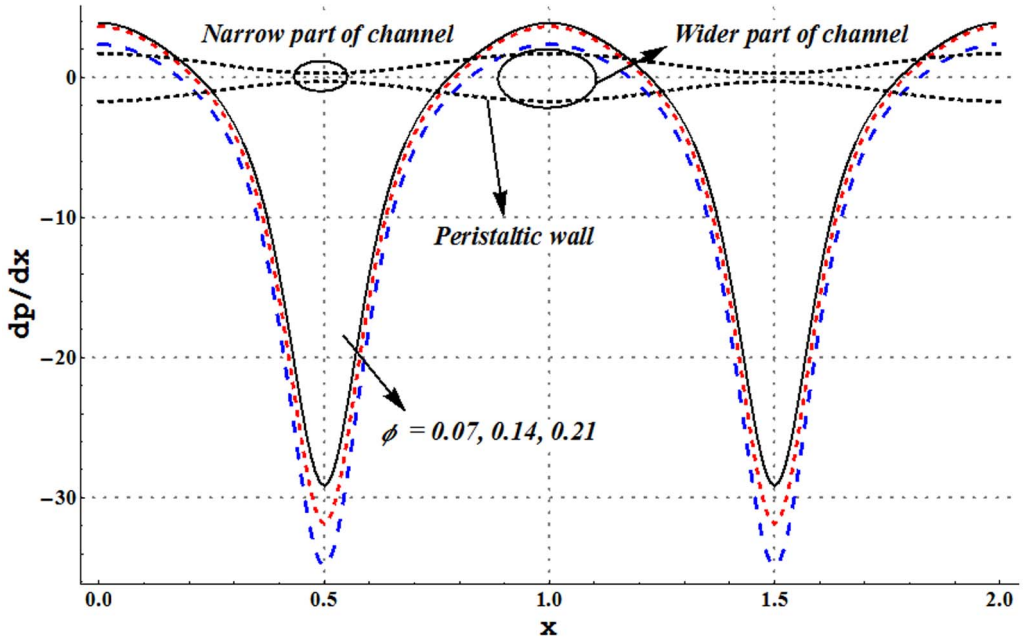

Figure 2. Pressure gradient for variation in nanoparticle volume fraction when $Gr=5$, $a=0.7$, $\eta=1.2$, $Br=0.3$, $\varepsilon=1.0$, $\beta=0.1$, $\gamma=0.1$ and $\alpha=\pi/4$.
doi:10.1371/journal.pone.0105440.g002

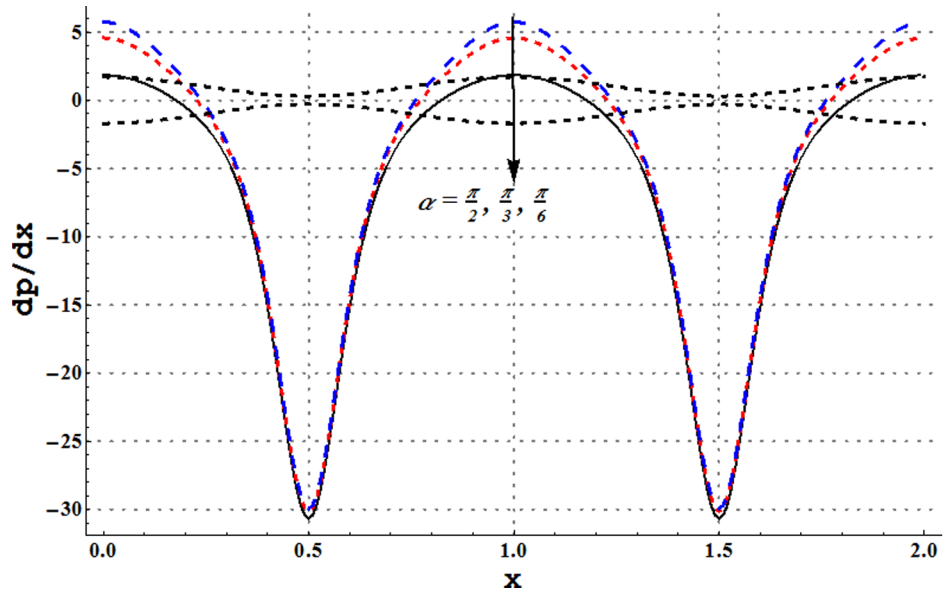

Figure 3. Pressure gradient for variation in channel inclination angle when $Gr=5$, $a=0.7$, $\eta=1.2$, $Br=0.3$, $\varepsilon=1.0$, $\beta=0.1$, $\gamma=0.1$ and $\phi=0.1$.
doi:10.1371/journal.pone.0105440.g003

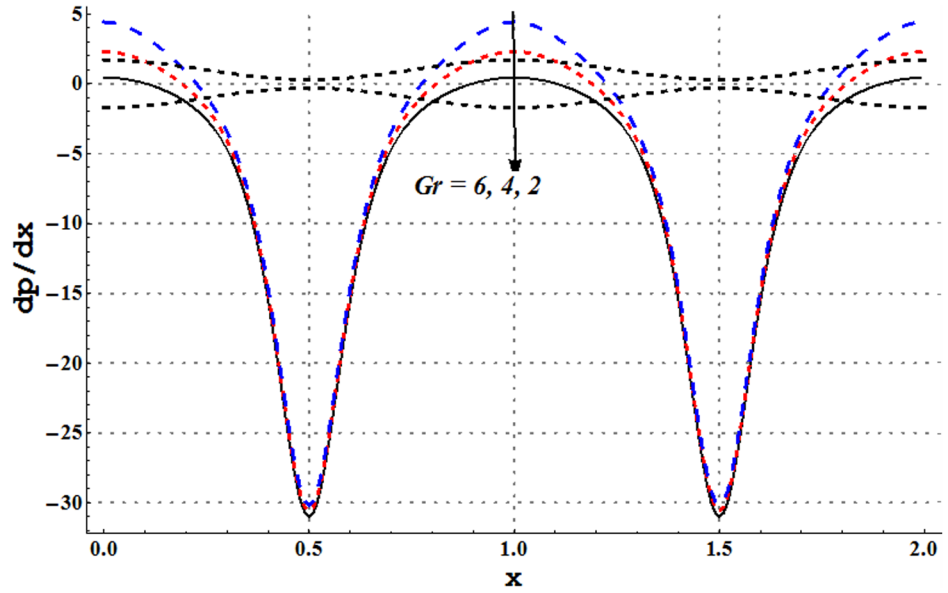

Figure 4. Pressure gradient for variation in Grashoff number when $\phi=0.1$, $a=0.7$, $\eta=1.2$, $Br=0.3$, $\varepsilon=1.0$, $\beta=0.1$, $\gamma=0.1$ and $\alpha=\pi/4$.
doi:10.1371/journal.pone.0105440.g004

$$\frac{\partial \overline{U}}{\partial \overline{X}}+\frac{\partial \overline{V}}{\partial \overline{Y}}=0, \tag{2}$$

where $\overline{U}$ and $\overline{V}$ are the longitudinal and transverse components of velocity in the laboratory frame. The $\overline{X}$ and $\overline{Y}$ components of momentum equation in presence of mixed convection are

$$\rho_{nf}\left(\frac{\partial}{\partial \overline{t}}+\overline{U}\frac{\partial}{\partial \overline{X}}+\overline{V}\frac{\partial}{\partial \overline{Y}}\right)\overline{U}=-\frac{\partial \overline{P}}{\partial \overline{X}}+\mu_{eff}\left(\frac{\partial^2 \overline{U}}{\partial \overline{X}^2}+\frac{\partial^2 \overline{U}}{\partial \overline{Y}^2}\right) +g(\rho\beta)_{nf}(T-T_0)\,\sin\alpha, \tag{3}$$

$$\rho_{nf}\left(\frac{\partial}{\partial \overline{t}}+\overline{U}\frac{\partial}{\partial \overline{X}}+\overline{V}\frac{\partial}{\partial \overline{Y}}\right)\overline{V}=-\frac{\partial \overline{P}}{\partial \overline{Y}}+\mu_{eff}\left(\frac{\partial^2 \overline{V}}{\partial \overline{X}^2}+\frac{\partial^2 \overline{V}}{\partial \overline{Y}^2}\right) -g(\rho\beta)_{nf}(T-T_0)\,\cos\alpha. \tag{4}$$

Energy equation with viscous dissipation and heat generation/absorption is given by

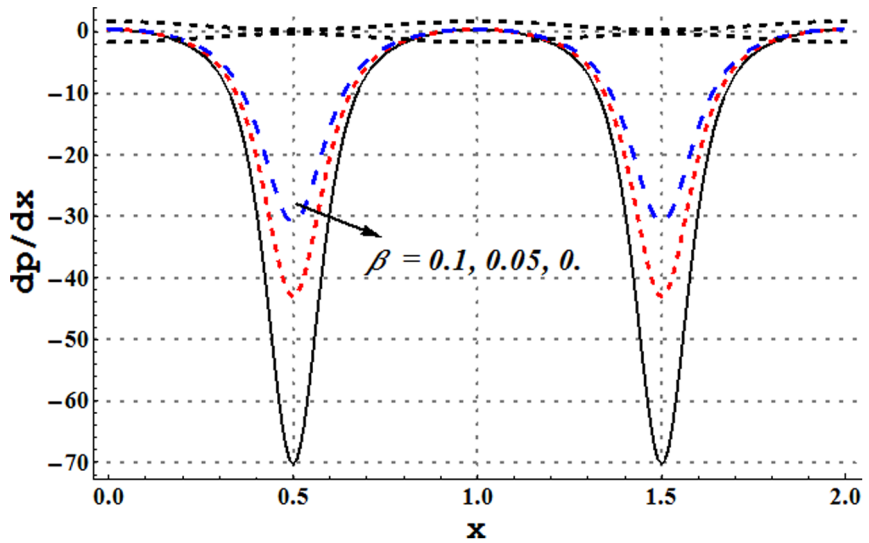

Figure 5. Pressure gradient for variation in velocity slip parameter when $Gr=5$, $a=0.7$, $\eta=1.2$, $Br=0.3$, $\varepsilon=1.0$, $\phi=0.1$, $\gamma=0.1$ and $\alpha=\pi/4$.
doi:10.1371/journal.pone.0105440.g005

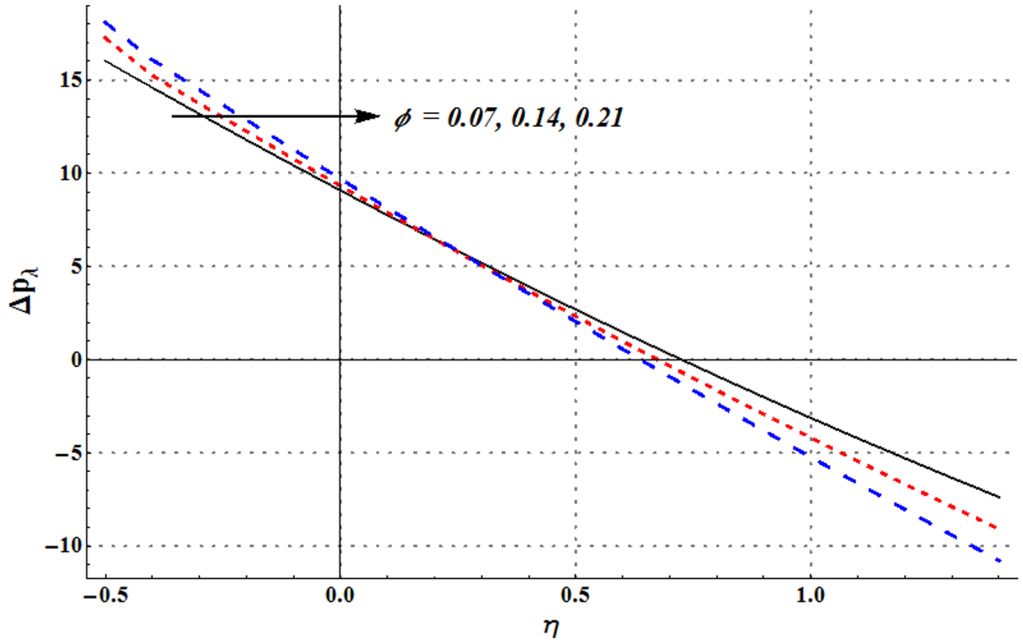

Figure 6. Pressure rise per wavelength for change in nanoparticle volume fraction when $Gr=5$, $a=0.7$, $Br=0.3$, $\varepsilon=1.0$, $\beta=0.1$, $\gamma=0.1$ and $\alpha=\pi/4$.
doi:10.1371/journal.pone.0105440.g006

$$(\rho C)_{nf}\left(\frac{\partial}{\partial \overline{t}}+\overline{U}\frac{\partial}{\partial \overline{X}}+\overline{V}\frac{\partial}{\partial \overline{Y}}\right)T=K_{eff}\left(\frac{\partial^2 T}{\partial \overline{X}^2}+\frac{\partial^2 T}{\partial \overline{Y}^2}\right)+\Phi$$
$$+\mu_{eff}\left[2\left(\left(\frac{\partial \overline{U}}{\partial \overline{X}}\right)^2+\left(\frac{\partial \overline{V}}{\partial \overline{Y}}\right)^2\right)+\left(\frac{\partial \overline{U}}{\partial \overline{Y}}+\frac{\partial \overline{V}}{\partial \overline{X}}\right)^2\right]. \quad (5)$$

In these equations $\overline{P}$ is the pressure in laboratory frame, μ_{eff} the effective viscosity of nanofluid, ρ_{nf} the density of nanofluid, β_{nf} thermal expansion coefficient of the nanofluid, g the acceleration due to gravity, T the fluid temperature, C_{nf} the specific heat of nanofluid, K_{eff} the effective thermal conductivity of nanofluid and Φ the dimensional heat source/sink parameter. Nomenclature of all the quantities is also provided through Table 1. Effective viscosity of the nanofluid can be computed with the help of

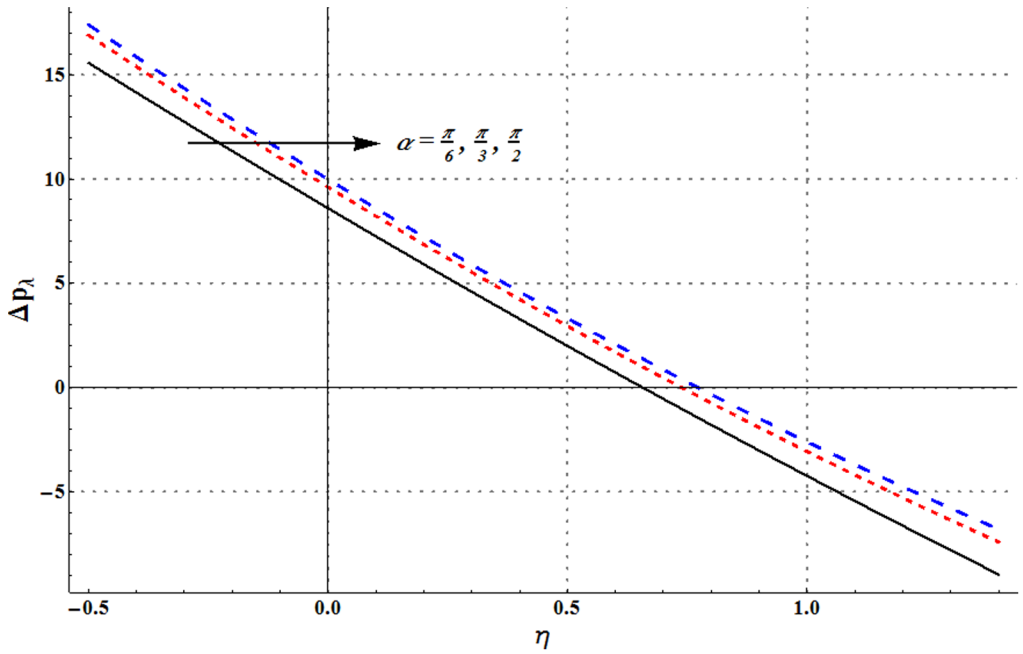

Figure 7. Pressure rise per wavelength for change in channel inclination when $Gr=5$, $a=0.7$, $Br=0.3$, $\varepsilon=1.0$, $\beta=0.1$, $\gamma=0.1$ and $\phi=0.1$.
doi:10.1371/journal.pone.0105440.g007

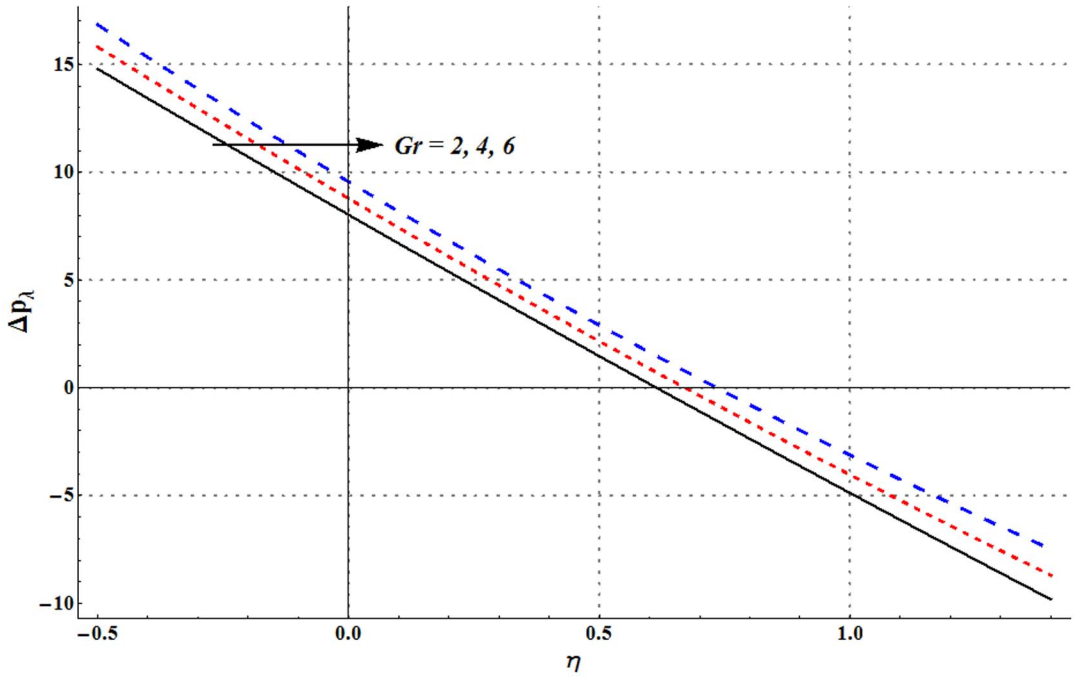

Figure 8. Pressure rise per wavelength for change in Grashoff number when $\phi=0.1$, $a=0.7$, $Br=0.3$, $\varepsilon=1.0$, $\beta=0.1$, $\gamma=0.1$ and $\alpha=\pi/4$.
doi:10.1371/journal.pone.0105440.g008

equations for two-phase flow. In this study we have used the relation proposed by Brinkman [7]

$$\mu_{eff}=\frac{\mu_f}{(1-\phi)^{2.5}}. \tag{6}$$

Relations for effective density, specific heat and thermal conductivity of nanofluid by Tiwari and Das [9] are

$$\rho_{nf}=(1-\phi)\rho_f+\phi\rho_p,\ (\rho C)_{nf}=((1-\phi)(C\rho)_f+\phi(C\rho)_p),$$
$$(\rho\beta)_{nf}=(1-\phi)\rho_f\beta_f+\phi\beta_p\rho_p,\ \frac{K_{eff}}{K_f}=\frac{K_p+2K_f-2\phi(K_f-K_p)}{K_p+2K_f+\phi(K_f-K_p)}. \tag{7}$$

Here Maxwell-Gamett's (MG-model) is used to approximate the effective thermal conductivity of the nanofluid. In these equations ϕ denotes the nanoparticle volume fraction, ρ_f the density of base

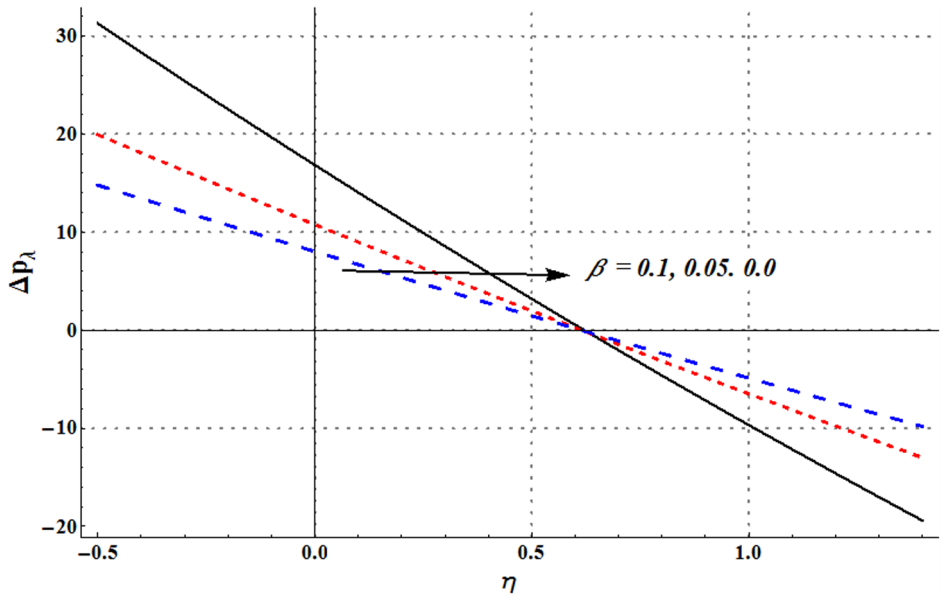

Figure 9. Pressure rise per wavelength for change in velocity slip parameter when $Gr=5$, $a=0.7$, $Br=0.3$, $\varepsilon=1.0$, $\phi=0.1$, $\gamma=0.1$ and $\alpha=\pi/4$.
doi:10.1371/journal.pone.0105440.g009

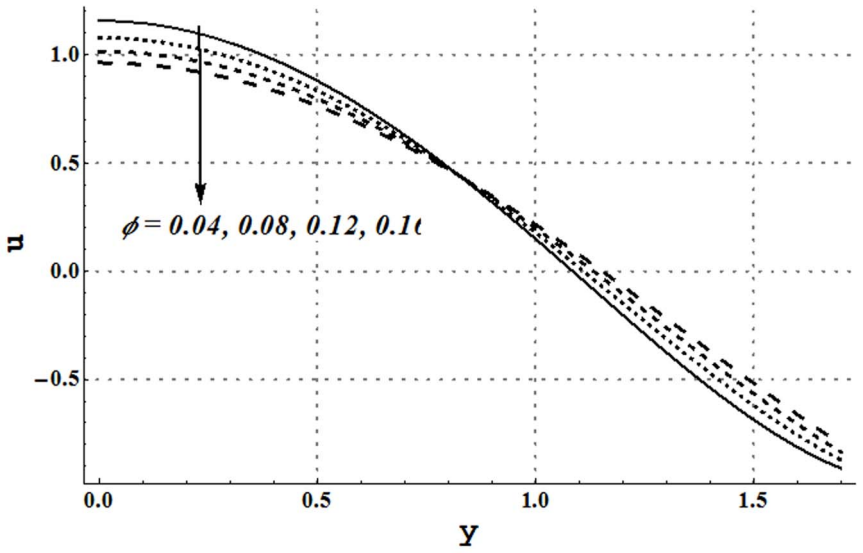

Figure 10. Axial velocity for different nanoparticle volume fraction when $Gr=5$, $a=0.7$, $x=1$, $\eta=1.5$, $Br=0.3$, $\varepsilon=1.0$, $\beta=0.1$, $\gamma=0.1$ and $\alpha=\pi/4$.
doi:10.1371/journal.pone.0105440.g010

fluid (water in this case), ρ_p the density of nanoparticles, β_f the thermal expansion coefficient of base fluid, β_p the thermal expansion of nanoparticles, μ_f the viscosity of base fluid, K_p the thermal conductivity of nanoparticles and K_f the thermal conductivity of base fluid. Numerical values of these properties are readily available which we include in the Table 2 [9,10].

The quantities from the laboratory frame $(\overline{X}, \overline{Y}, \overline{t})$ to wave frame $(\overline{x}, \overline{y})$ are related by the following transformations:

$$\overline{x}=\overline{X}-c\overline{t}, \overline{y}=\overline{Y}, \overline{u}=\overline{U}-c, \overline{v}=\overline{V}, \overline{p}(\overline{x},\overline{y})=\overline{P}(\overline{X},\overline{Y},\overline{t}), \quad (8)$$

in which $\overline{u}$, $\overline{v}$ and $\overline{p}$ are the velocity components and pressure in wave frame $(\overline{x}, \overline{y})$. Equations (2)–(5) through Eqs. (6–8) yield

$$\frac{\partial \overline{u}}{\partial \overline{x}}+\frac{\partial \overline{v}}{\partial \overline{y}}=0, \quad (9)$$

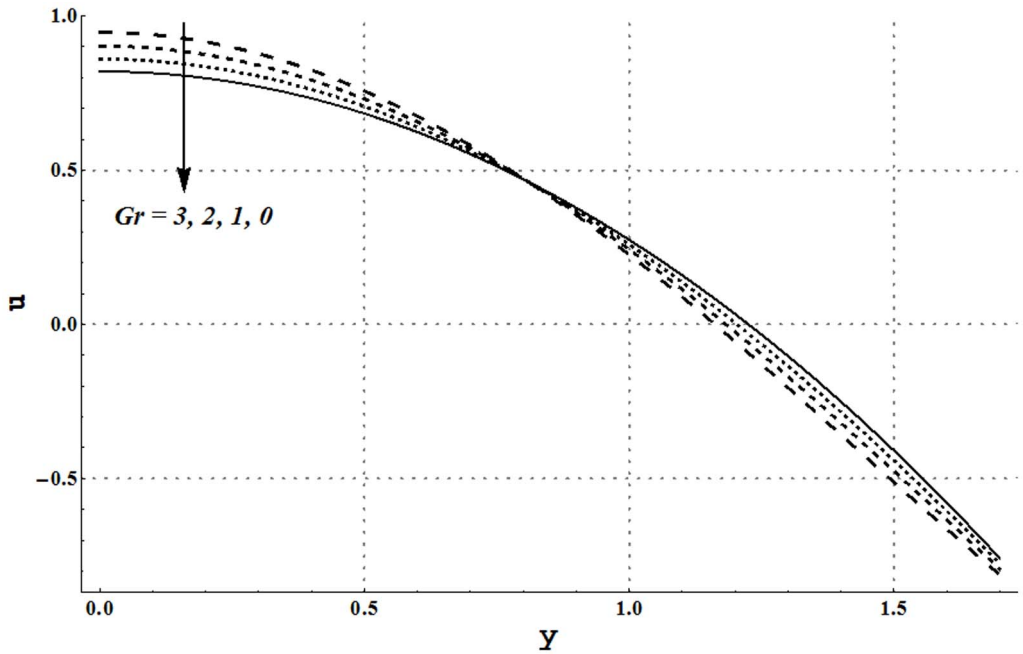

Figure 11. Axial velocity for different Grashoff numbers when $\phi=0.1$, $a=0.7$, $x=1$, $\eta=1.5$, $Br=0.3$, $\varepsilon=1.0$, $\beta=0.1$, $\gamma=0.1$ and $\alpha=\pi/4$.
doi:10.1371/journal.pone.0105440.g011

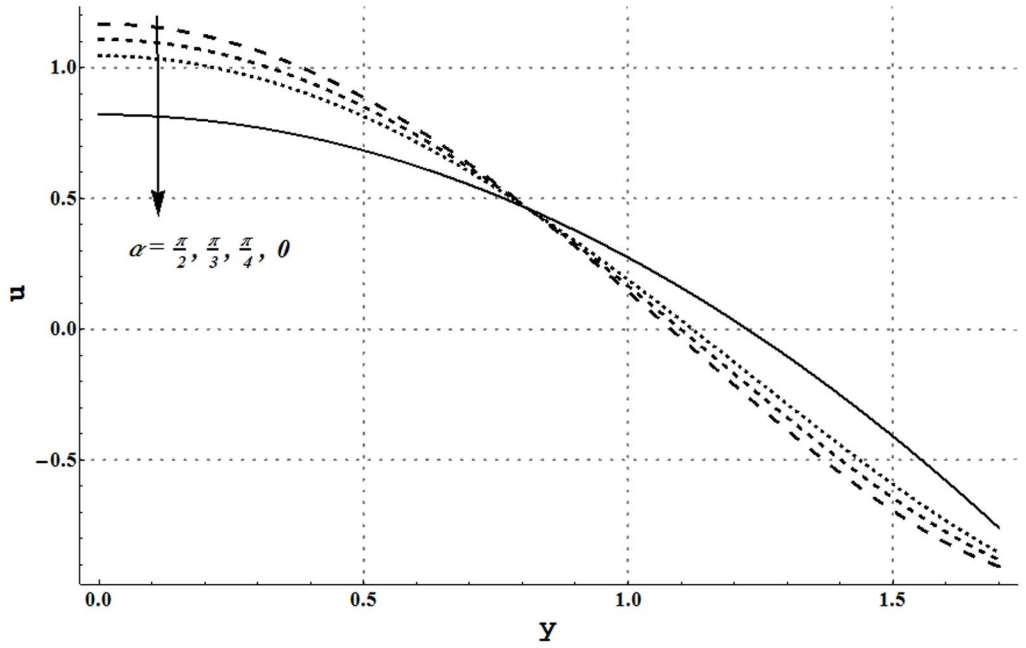

Figure 12. Axial velocity for different inclination angles when $Gr = 5$, $a = 0.7$, $x = 1$, $\eta = 1.5$, $Br = 0.3$, $\varepsilon = 1.0$, $\beta = 0.1$, $\gamma = 0.1$ and $\phi = 0.1$.
doi:10.1371/journal.pone.0105440.g012

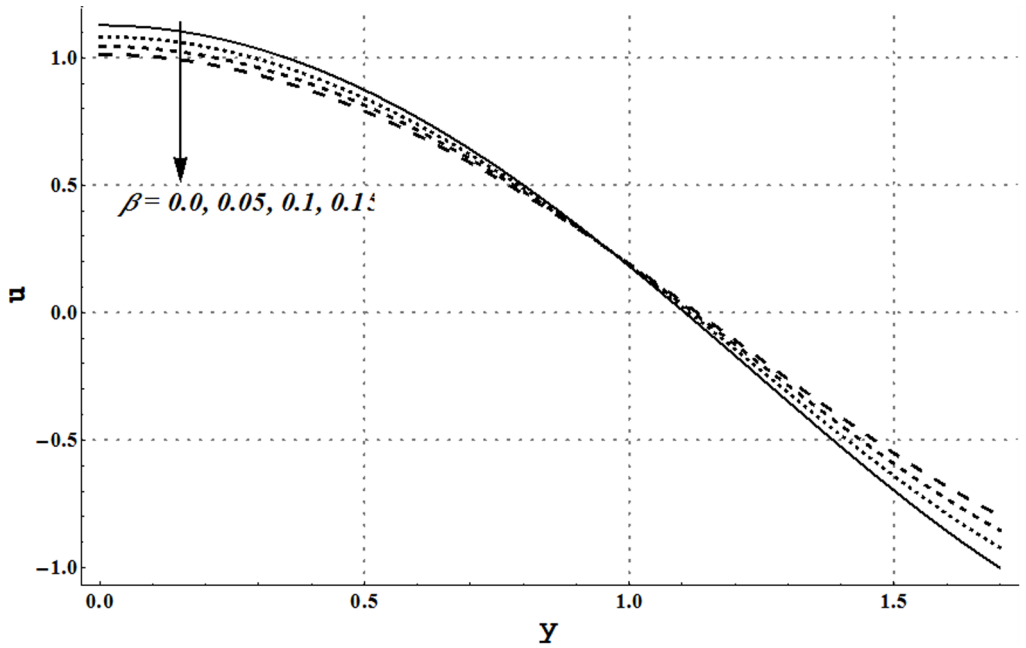

Figure 13. Axial velocity for different values of velocity slip parameter when $Gr = 5$, $a = 0.7$, $x = 1$, $\eta = 1.5$, $Br = 0.3$, $\varepsilon = 1.0$, $\phi = 0.1$, $\gamma = 0.1$ and $\alpha = \pi/4$.
doi:10.1371/journal.pone.0105440.g013

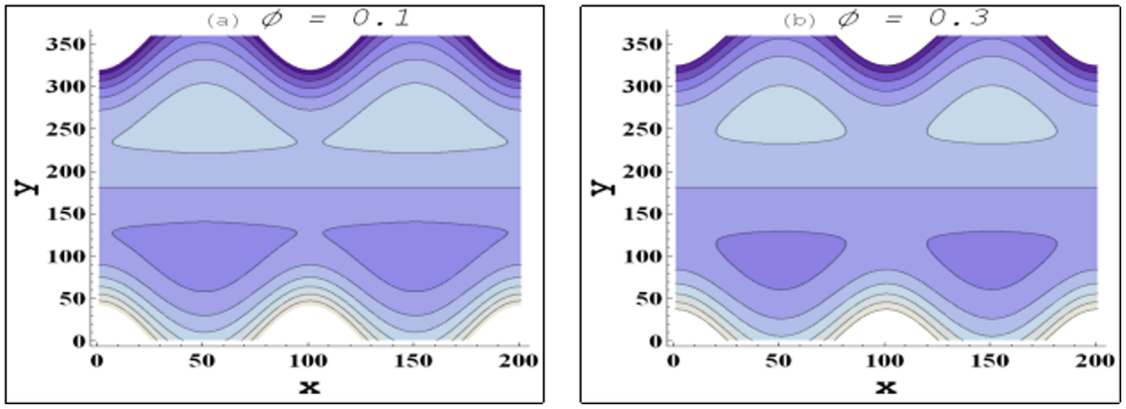

Figure 14. Behavior of streamlines for variation in nanoparticle volume fraction when $Gr=5$, $a=0.7$, $\eta=1.5$, $Br=0.3$, $\varepsilon=1.0$, $\beta=0.1$, $\gamma=0.1$ and $\alpha=\pi/4$.
doi:10.1371/journal.pone.0105440.g014

$$((1-\phi)\rho_f+\phi\rho_p)\left((\overline{u}+c)\frac{\partial}{\partial\overline{x}}+\overline{v}\frac{\partial}{\partial\overline{Y}}\right)(\overline{u}+c)$$
$$=-\frac{\partial\overline{p}}{\partial\overline{x}}+\frac{\mu_f}{(1-\phi)^{2.5}}\left(\frac{\partial^2\overline{u}}{\partial\overline{x}^2}+\frac{\partial^2\overline{u}}{\partial\overline{y}^2}\right) \quad (10)$$
$$+g\left((1-\phi)\rho_f\beta_f+\phi\beta_p\rho_p\right)(T-T_0)\sin\alpha,$$

$$((1-\phi)\rho_f+\phi\rho_p)\left((\overline{u}+c)\frac{\partial}{\partial\overline{x}}+\overline{v}\frac{\partial}{\partial\overline{Y}}\right)\overline{v}$$
$$=-\frac{\partial\overline{p}}{\partial\overline{y}}+\frac{\mu_f}{(1-\phi)^{2.5}}\left(\frac{\partial^2\overline{v}}{\partial\overline{x}^2}+\frac{\partial^2\overline{v}}{\partial\overline{y}^2}\right) \quad (11)$$
$$-g\left((1-\phi)\rho_f\beta_f+\phi\beta_p\rho_p\right)(T-T_0)\cos\alpha,$$

$$((1-\phi)(C\rho)_f+\phi(C\rho)_p)\left((\overline{u}+c)\frac{\partial}{\partial\overline{x}}+\overline{v}\frac{\partial}{\partial\overline{y}}\right)T$$
$$=K_{eff}\left(\frac{\partial^2T}{\partial\overline{x}^2}+\frac{\partial^2T}{\partial\overline{y}^2}\right)+\Phi \quad (12)$$
$$+\frac{\mu_f}{(1-\phi)^{2.5}}\left[2\left(\left(\frac{\partial\overline{u}}{\partial\overline{x}}\right)^2+\left(\frac{\partial\overline{v}}{\partial\overline{y}}\right)^2\right)+\left(\frac{\partial\overline{u}}{\partial\overline{y}}+\frac{\partial\overline{v}}{\partial\overline{x}}\right)^2\right].$$

With the help of following dimensionless quantities

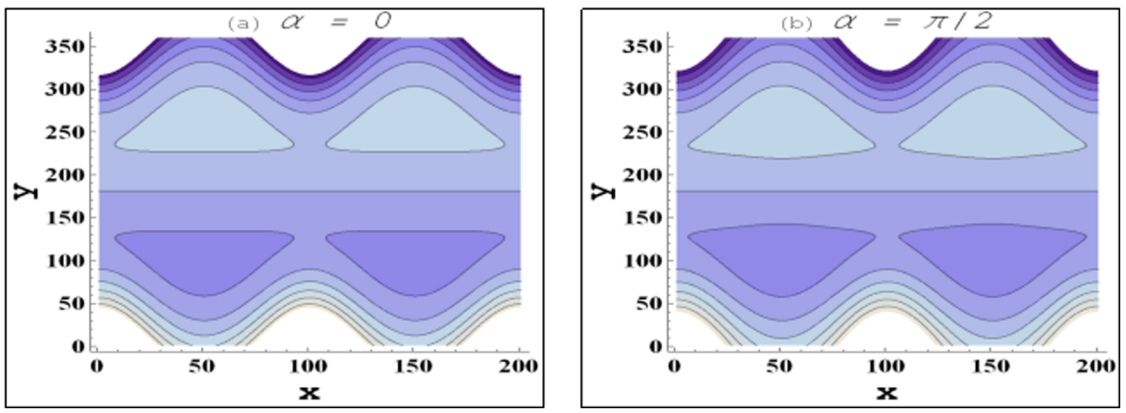

Figure 15. Behavior of streamlines for variation in channel inclination when $Gr=5$, $a=0.7$, $\eta=1.5$, $Br=0.3$, $\varepsilon=1.0$, $\beta=0.1$, $\gamma=0.1$ and $\phi=0.1$.
doi:10.1371/journal.pone.0105440.g015

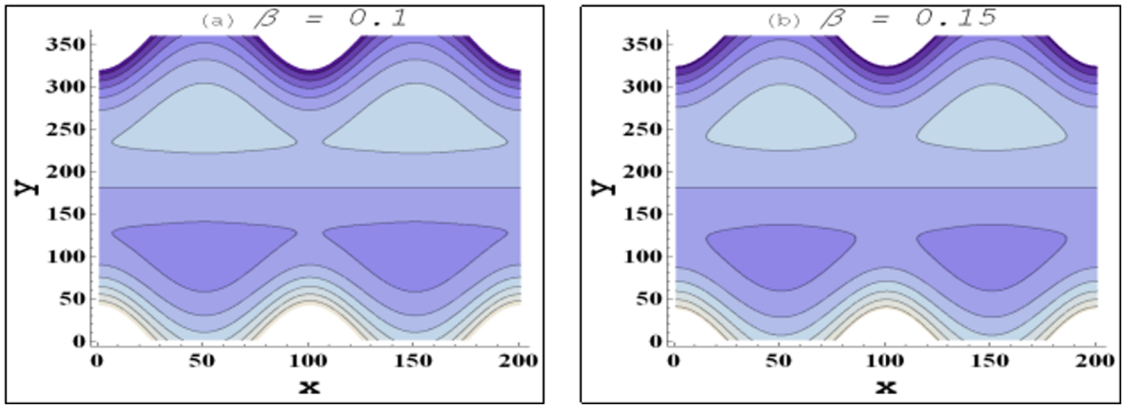

Figure 16. Behavior of streamlines for variation in velocity slip parameter when $Gr=5$, $a=0.7$, $\eta=1.5$, $Br=0.3$, $\varepsilon=1.0$, $\phi=0.1$, $\gamma=0.1$ and $\alpha=\pi/4$.
doi:10.1371/journal.pone.0105440.g016

$$
\begin{aligned}
&x=\frac{\overline{x}}{\lambda}, y=\frac{\overline{y}}{d}, u=\frac{\overline{u}}{c}, v=\frac{\overline{v}}{c\delta}, \delta=\frac{d}{\lambda}, h=\frac{\overline{H}}{d}, a=\frac{a_1}{d},\\
&p=\frac{d^2\overline{p}}{c\lambda\mu_f}, \theta=\frac{T-T_0}{T_0}, \upsilon=\frac{\mu_f}{\rho_f}, \mathrm{Re}=\frac{\rho_f cd}{\mu_f},\\
&t=\frac{c\overline{t}}{\lambda}, E=\frac{c^2}{C_f T_0}, \mathrm{Pr}=\frac{\mu_f C_f}{K_f}, Gr=\frac{\rho_f g\beta_f T_0 d^2}{\mu_f c},\\
&Br=\mathrm{Pr}E, \varepsilon=\frac{d^2\Phi}{T_0K_f}, u=\frac{\partial\psi}{\partial y}, v=-\frac{\partial\psi}{\partial x},
\end{aligned}
\tag{13}
$$

and applying the long wavelength and low Reynolds number approximations Eqs. (10–12) are reduced to the following expressions:

$$
\frac{\partial p}{\partial x}=\frac{1}{(1-\phi)^{2.5}}\frac{\partial^3\psi}{\partial y^3}+Gr\sin\alpha\left\{1-\phi+\phi\left(\frac{(\rho\beta)_p}{(\rho\beta)_f}\right)\right\}\theta, \tag{14}
$$

$$
p_y=0, \tag{15}
$$

$$
\frac{K_p+2K_f-2\phi(K_f-K_p)}{K_p+2K_f+\phi(K_f-K_p)}\frac{\partial^2\theta}{\partial y^2}+\frac{Br}{(1-\phi)^{2.5}}\left(\frac{\partial^2\psi}{\partial y^2}\right)^2+\varepsilon=0. \tag{16}
$$

where the continuity equation is identically satisfied and Eq. (15)

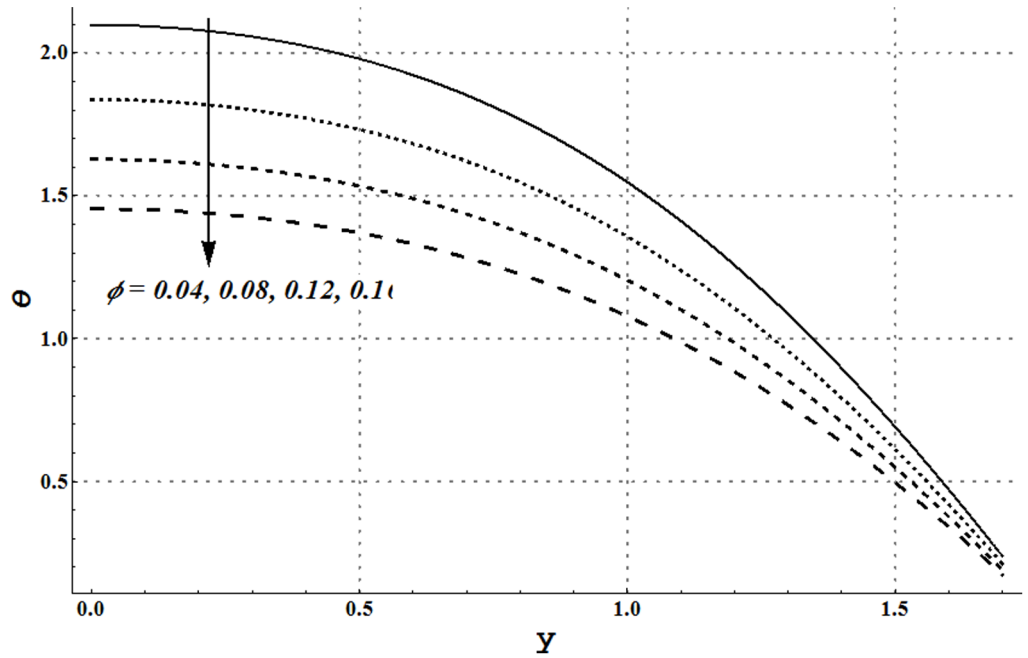

Figure 17. Temperature profile for different nanoparticle volume fractions when $Gr=5$, $a=0.7$, $x=1$, $\eta=1.5$, $Br=0.3$, $\varepsilon=1.0$, $\beta=0.1$, $\gamma=0.1$ and $\alpha=\pi/4$.
doi:10.1371/journal.pone.0105440.g017

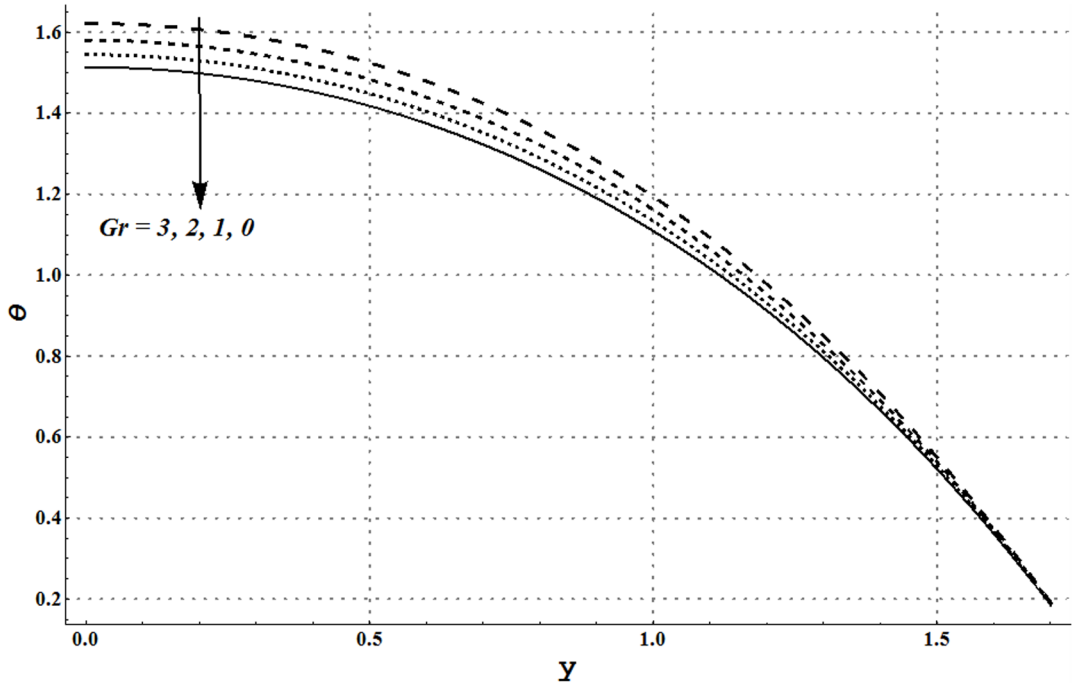

Figure 18. Temperature profile for variation in Grashoff number when $\phi=0.1$, $a=0.7$, $x=1$, $\eta=1.5$, $Br=0.3$, $\varepsilon=1.0$, $\beta=0.1$, $\gamma=0.1$ and $\alpha=\pi/4$.
doi:10.1371/journal.pone.0105440.g018

shows that $p \neq p(y)$. In these equations ψ is the stream function, *Re* the Reynolds number, *Br* the Brinkman number, *E* the Eckret number, Pr the Prandtl number, δ the wave number, θ the dimensionless temperature and ε the dimensionless heat source/sink parameter. From Eqs. 14 and 15 one obtains

$$0=\frac{1}{(1-\phi)^{2.5}}\frac{\partial^4\psi}{\partial y^4}+Gr\sin\alpha\left\{1-\phi+\phi\left(\frac{(\rho\beta)_p}{(\rho\beta)_f}\right)\right\}\frac{\partial\theta}{\partial y}. \quad (17)$$

Defining η and F as the dimensionless mean flows in laboratory and wave frames by

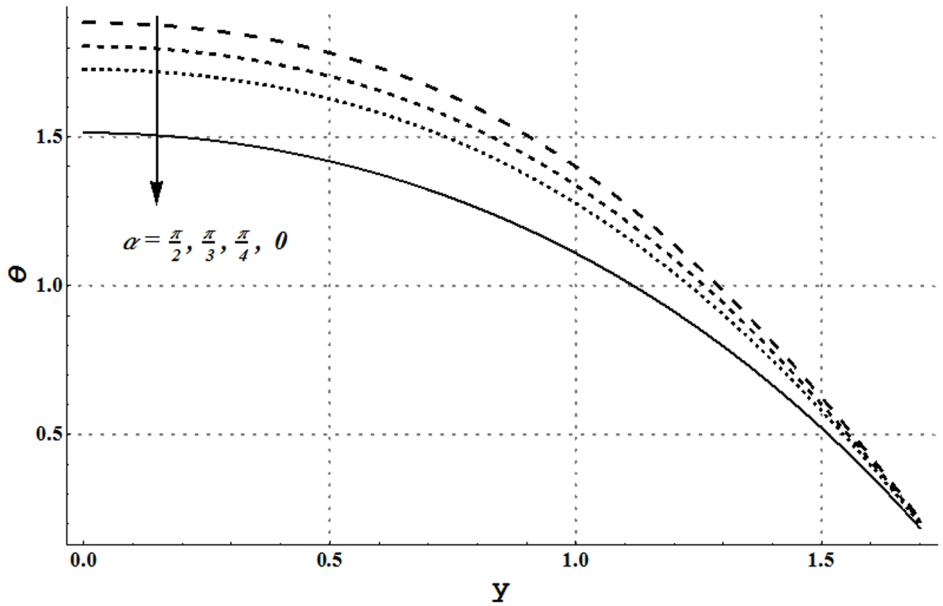

Figure 19. Temperature profile for variation in channel inclination angle when $Gr=5$, $a=0.7$, $x=1$, $\eta=1.5$, $Br=0.3$, $\varepsilon=1.0$, $\beta=0.1$, $\gamma=0.1$ and $\phi=0.1$.
doi:10.1371/journal.pone.0105440.g019

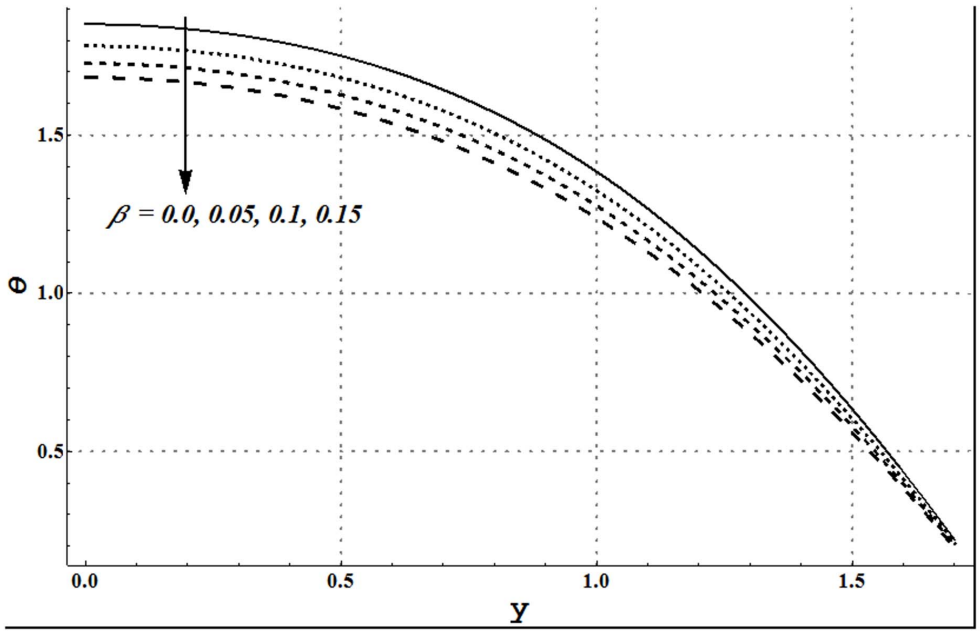

Figure 20. Temperature profile for variation in velocity slip parameter when $Gr=5$, $a=0.7$, $x=1$, $\eta=1.5$, $Br=0.3$, $\varepsilon=1.0$, $\phi=0.1$, $\gamma=0.1$ and $\alpha=\pi/4$.
doi:10.1371/journal.pone.0105440.g020

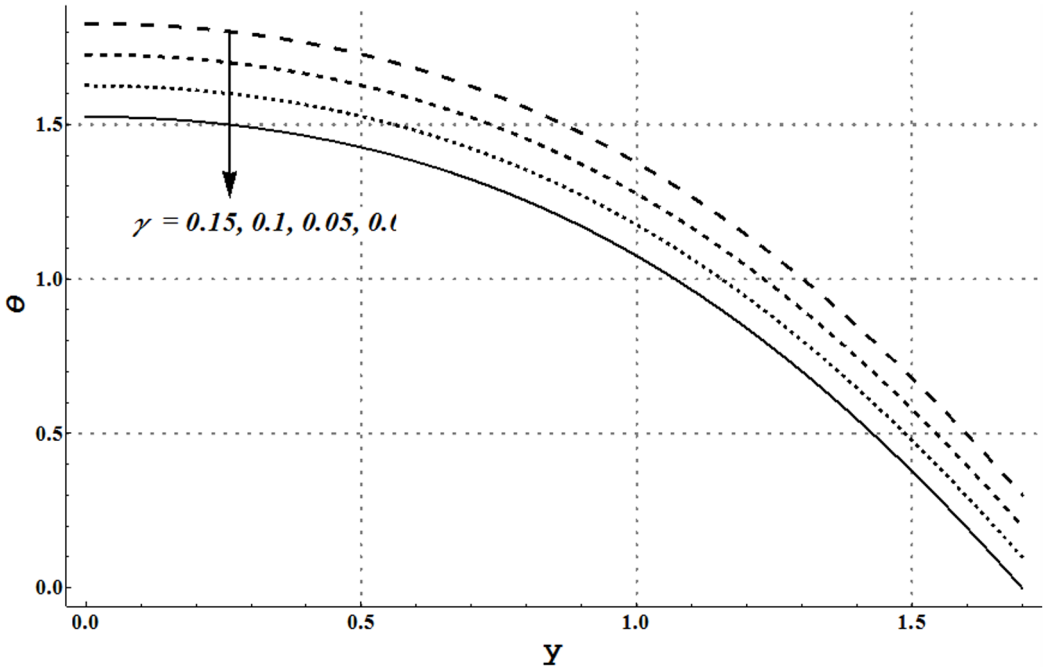

Figure 21. Temperature profile for variation in thermal slip parameter when $Gr=5$, $a=0.7$, $x=1$, $\eta=1.5$, $Br=0.3$, $\varepsilon=1.0$, $\beta=0.1$, $\phi=0.1$ and $\alpha=\pi/4$.
doi:10.1371/journal.pone.0105440.g021

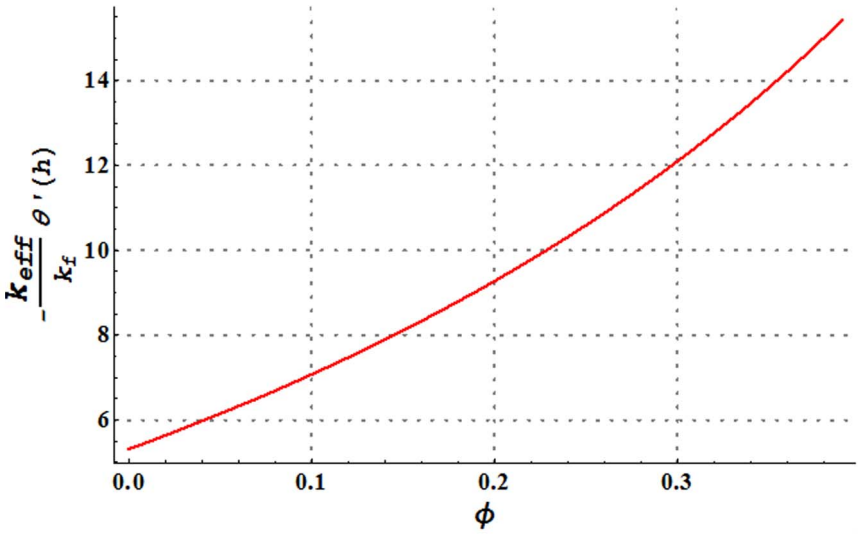

Figure 22. Change in heat transfer rate at the wall for variation in nanoparticle volume fraction $Gr=5$, $a=0.7$, $x=1$, $\eta=1.5$, $Br=0.3$, $\varepsilon=1.0$, $\beta=0.1$, $\gamma=0.1$ and $\alpha=\pi/4$.
doi:10.1371/journal.pone.0105440.g022

$$\eta=\frac{\overline{Q}}{cd},F=\frac{\overline{q}}{cd} \tag{18}$$

two flow rates can be related as follows:

$$\eta=F+1, \tag{19}$$

where

$$F=\int_0^h \frac{\partial\psi}{\partial y}dy. \tag{20}$$

The velocity and thermal slip conditions are

$$\overline{U}-\overline{U}_w=\widehat{n}\beta_1\overline{\tau}_{xy},\ \overline{T}-\overline{T}_w=\widehat{n}\gamma_1\frac{\partial\overline{T}}{\partial y},$$

where $\overline{U}$ is the velocity of fluid, $\overline{\tau}_{xy}$ the component of extra stress tensor, $\overline{T}$ the temperature of fluid, β_1, γ_1 are respectively the dimensional velocity and thermal slip parameters and $\widehat{n}$ the unit normal on the wall. The dimensionless velocity and thermal slip conditions finally become

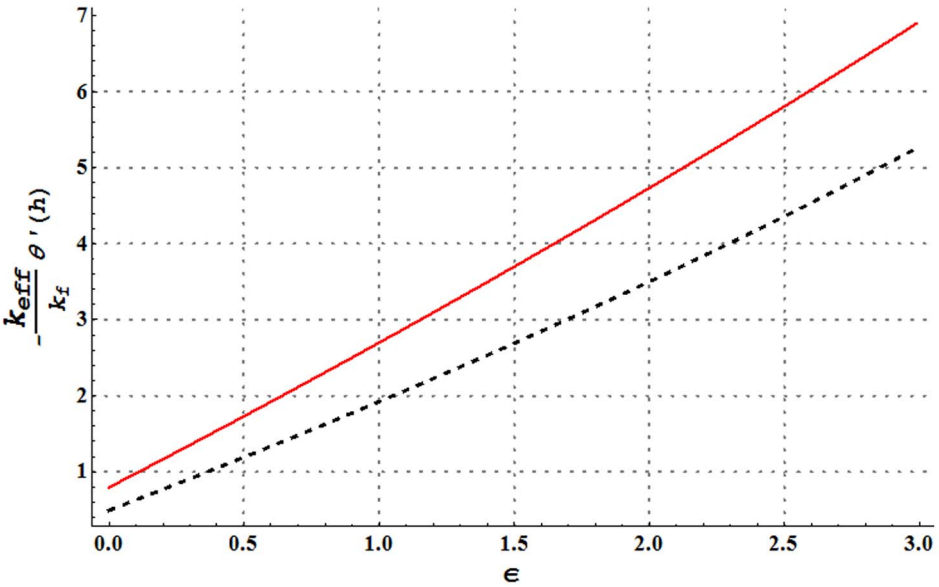

Figure 23. Comparison of heat transfer rate at the wall of water and Cu-water nanofluid for change in heat source/sink parameter when $Gr=5$, $a=0.7$, $x=1$, $\eta=1.5$, $Br=0.3$, $\beta=0.1$, $\gamma=0.1$ and $\alpha=\pi/4$.
doi:10.1371/journal.pone.0105440.g023

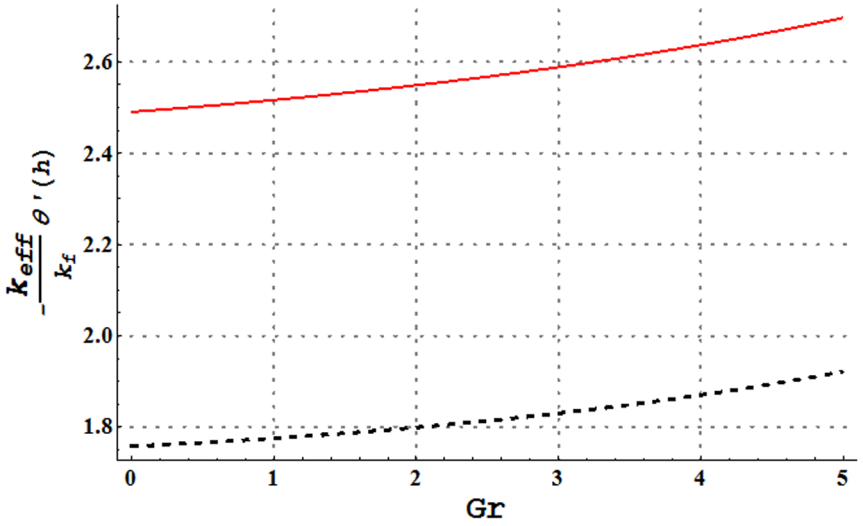

Figure 24. Comparison of heat transfer rate at the wall of water and Cu-water nanofluid for change in Grashoff number when $a=0.7$, $x=1$, $\eta=1.5$, $Br=0.3$, $\varepsilon=1.0$, $\beta=0.1$, $\gamma=0.1$ and $\alpha=\pi/4$.
doi:10.1371/journal.pone.0105440.g024

$$\frac{\partial\psi}{\partial y}+\frac{\beta}{(1-\phi)^{2.5}}\frac{\partial^2\psi}{\partial y^2}=-1,\theta+\gamma\frac{\partial\theta}{\partial y}=0,$$

where $\beta(=\frac{\mu_f\beta_1}{d})$ and $\gamma(=\frac{\gamma_1}{d})$ are respectively the dimensionless velocity and thermal slip pramaeters. The appropriate boundary conditions for the present flow model are

$$\begin{aligned}&\psi=0,\psi_{yy}=0,\theta_y=0,at\ y=0,\\&\psi=F,\frac{\partial\psi}{\partial y}+\frac{\beta}{(1-\phi)^{2.5}}\frac{\partial^2\psi}{\partial y^2}=-1,\theta+\gamma\frac{\partial\theta}{\partial y}=0,at\ y=h.\end{aligned}\tag{21}$$

with $h=1+a\cos(2\pi x)$. Pressure rise per wavelength (Δp_λ) is defined as follows:

$$\Delta p_\lambda=\int_0^1(\frac{dp}{dx})dx$$

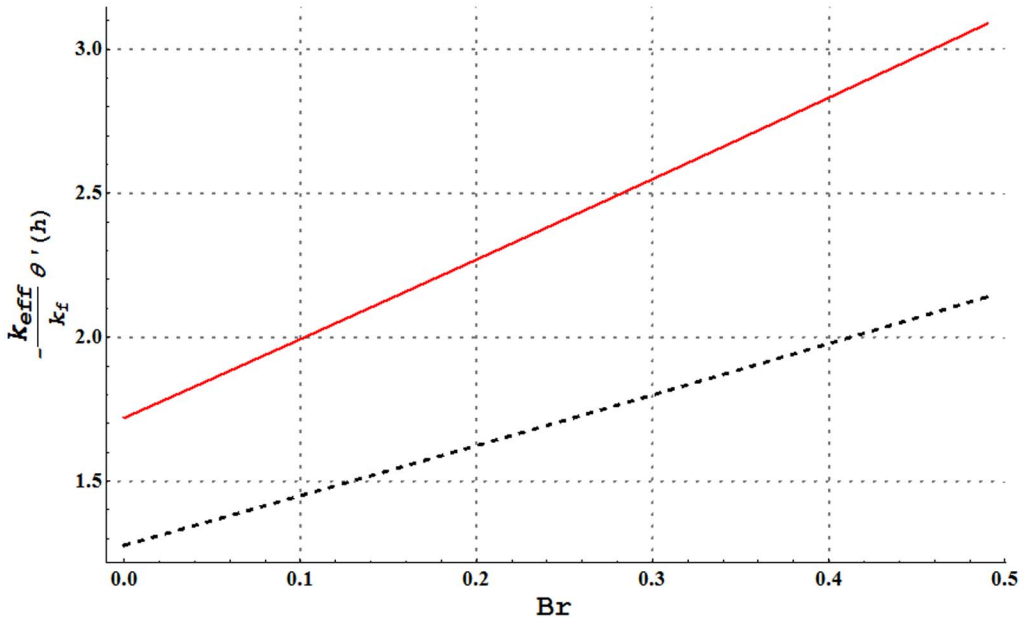

Figure 25. Comparison of heat transfer rate at the wall of water and Cu-water nanofluid for change in Brinkman number when $Gr=5$, $a=0.7$, $x=1$, $\eta=1.5$, $\varepsilon=1.0$, $\beta=0.1$, $\gamma=0.1$ and $\alpha=\pi/4$.
doi:10.1371/journal.pone.0105440.g025

Table 3. Numerical values of heat transfer rate at the wall for change in the values of different parameters when $Gr=5$, $a=0.7$, $x=1$, $\eta=1.5$, $Br=0.3$ and $\gamma=0.1$.

β	α	ε	$-\frac{k_{eff}}{k_f}\theta'(h)$
0.0	$\pi/4$	1.0	2.93204
0.05			2.79028
0.10			2.67728
0.15			2.58574
0.10	$\pi/6$		2.46308
	$\pi/4$		2.67727
	$\pi/3$		2.76587
	$\pi/2$		2.86097
	$\pi/4$	0.0	0.78554
		1.0	2.67227
		2.0	4.70860
		3.0	4.90948

doi:10.1371/journal.pone.0105440.t003

The system of Eqs. (14–16) subject to boundary conditions (21) is solved numerically using NDSolve in Mathematica. We have taken the step size equal to 0.01 for the variations in both variables x and y. Obtained numerical results are analyzed graphically in the next section.

Results and Discussion

Pressure gradient, pressure rise per wavelength, axial velocity and trapping are important quantities in the study of peristalsis. On the other hand the analysis of heat transfer phenomena is significant in the study of nanofluids. Hence the present section is prepared to analyze the behavior of pressure gradient, pressure rise per wavelength, axial velocity, streamlines, temperature and heat transfer rate at the wall for variation in different embedded parameters.

Pressure gradient and pressure rise pre wavelength

Pressure gradient is studied through Figs. 2–5. These Figs. show that pressure gradient is minimum in the occluded region of channel and attains maximum value in the wider part. Addition of copper nanoparticles reduces the pressure gradient. In addition an increase in the nanoparticle volume fraction decreases the pressure gradient. Such decrease is large in both the wider and occluded regions (see Fig. 2). Fig. 3 depicts that there is an increase in pressure gradient near the wider part of channel when inclinations increases. Effect of Grashoff number on pressure gradient is similar to that of channel inclination angle (see Fig. 4). Pressure gradient enhances when the velocity slip parameter is increased (see Fig. 5). Such increase is large in the occluded portion of the channel.

Pressure rise per wavelength versus flow rate is shown in the Figs. 6–9. One common observation from these Figs. is that pressure rise per wavelength decreases with an increase in the flow rate. Fig. 6 shows that addition of nanoparticles decreases the free pumping flux (value of η for $\Delta p_\lambda=0$). Moreover an increase in the value of nanoparticle volume fraction enhances the pressure rise in retrograde pumping region ($\eta<0,\ \Delta p_\lambda>0$). However reverse situation is seen in the augumented pumping region ($\eta>0$, $\Delta p_\lambda<0$). Figs. 7 and 8 show that increase in the values of Grashoff number and channel inclination angle result in the increase of pressure rise per wavelength. Fig. 9 shows that large velocity slip parameter decreases the peristaltic pumping region ($\eta>0$, $\Delta p_\lambda>0$). Value of pressure rise per wavelength decreases largely in the retrograde pumping region when β increases.

Axial velocity and trapping phenomena

Effects of several flow parameters on axial velocity are shown in Figs. 10–13. These Figs. show that velocity profile traces a parabolic trajectory with maximum value at the center of the channel. Fig. 10 depicts that nanofluid with low concentration of nanoparticles possesses higher value of the velocity at the center. Which concluded that higher nanoparticles volume fraction provides more resistance to the flow. However near the channel walls, this observation is not true which primarily is due to slip effects. Figs. 11 and 12 show that increase in Grashoff number and channel inclination angle result in an increase in velocity at the center. As in previous case this observation is also reversed near the channel walls. Velocity near the channel walls increases with an increase in the velocity slip parameter (see Fig. 13). However maximum value of velocity at the center decreases subject to an increase in β.

Table 4. Comparison of present study with the results obtained by obtained by Ali et al [28] when $a=0.6$ and $\beta=0.02$.

	Alit et al. [28]	Present study for $Gr=0$, $\phi=0$
Critical value of η for Δp_λ	0.45022	0.45233405
Critical value of η for F_λ	0.3501	0.3505850

doi:10.1371/journal.pone.0105440.t004

Trapping for different involved parameters is studied through Figs. 14–16. Some volume of fluid during flow tends to get trapped within streamlines. This phenomenon is usually known as trapping and the volume of fluid thus trapped is named as bolus. Size of such bolus reduces with an increase in the value of nanoparticle volume fraction (see Fig. 14). Hence it can be stated that addition of nanoparticles reduces the trapping. Size of the trapped bolus slightly increases with an increase in the channel inclination angle (see Fig. 15). Fig. 16 depicts that size of the trapped bolus reduces with an increase in the velocity slip parameter.

Heat transfer analysis

Impact of several embedded parameters on temperature and heat transfer rate at the wall are examined through Figs. 17–25. It is clear from Fig. 17 that an increase in the nanoparticle volume fraction shows a decrease in fluid temperature. This clearly witnesses that the heat being generated by the heat source is quickly transferred to the walls (due to addition of more nanoparticles) and consequently the fluid temperature decreases. High thermal conductivity of nanoparticles plays a key role in quick dissipation of the fluid temperature. This justifies the use of copper nanoparticles in different types as the coolants. Figs. 18 and 19 show that increase in the values of Grashoff number and channel inclination enhance the fluid temperature. This is due to the fact that increase in Gr and α facilitates the convective heat transfer within the fluid. Figs. 20 and 21 show that velocity and thermal slip parameters have opposite effects on temperature of cu-water nanofluid. Temperature of nanofluid decreases with an increase in the velocity slip parameter.

Heat transfer rate at the wall for variation in nanoparticle volume fraction is analyzed in Fig. 22. It is observed that larger nanoparticle volume fraction increases the heat transfer rate at the wall. Hence addition of copper nanoparticles facilitates the heat transfer between the fluid and solid boundary and ultimately preventing the fluid from heating. Figs. 23–25 present a comparison of the heat transfer rate at the wall of water in the absence and presence of copper nanoparticles. All these Figs. show that copper-water nanofluid possesses higher heat transfer rate at the wall when compared with ordinary water. Also heat transfer rate is seen to increase by increasing ε, Gr and Br. Numerical values of heat transfer rate at the wall for variations in β, α and ε are given in Table 3. It is observed that heat transfer rate at the wall increases when α and ε are increased. However it decreases through larger β. Comparison between the limiting case of present study and the analysis performed by Ali et al. [28] is provided through Table 4.Critical values of flow rate are provided and compared. Good comparison is found between the two.

Conclusions

Velocity and thermal slip effects on the peristaltic transport of copper-water nanofluid in an inclined channel are studied. Findings of present analysis indicate that the addition of copper nanoparticles reduces the pressure gradient. Increase in the value of nanoparticle volume fraction enhances the pressure rise in retrograde pumping region. Nanofluid with low concentration of copper nanoparticles possesses higher value of velocity at the center of channel. Velocity slip parameter has a decreasing effect on the maximum value of axial velocity. Trapping is reduced in presence of nanoparticles. Grashoff number and channel inclination angle have increasing effect on the temperature of nanofluid. Increase in nanoparticle volume fraction largely enhances the heat transfer rate at the wall.

Author Contributions

Conceived and designed the experiments: TH FMA BA GQC. Performed the experiments: TH FMA BA GQC. Analyzed the data: TH FMA BA GQC. Contributed reagents/materials/analysis tools: TH FMA BA GQC. Wrote the paper: TH FMA BA GQC.

References

1. Choi SUS (1995) Enhancing thermal conductivity of fluids with nanoparticles. In: D.A. Siginer, H.P. Wang (Eds.). Developments and Applications of Non-Newtonian Flows, FED-Vol. 231/MD-vol. 66, ASME J. Heat Transfer, New York, 99–105.
2. Buongiorno J (2005) Convective transport in nanofluids. ASME J. Heat Transfer 128: 240–250.
3. Rashidi MM, Bég OA, Asadi M, Rastegari MT (2012) DTM- Padé modeling of natural convective boundary layer flow of a nanofluid Past a vertical surface. Int J Thermal & Environmental Eng., 4: 13–24.
4. Rashidi MM, Freidoonimehr N, Hosseini A, Bég OA, Hung TK (2014) Homotopy simulation of nanofluid dynamics from a non-linearly stretching isothermal permeable sheet with transpiration. Meccanica 49: 469–482.
5. Mustafa M, Farooq MA, Hayat T, Alsaedi A (2013) Numerical and series solutions for stagnation-point flow of nanofluid over an exponentially stretching sheet. PLOS ONE 8 (5): e61859.
6. Xuan Y, Li Q (2003) Investigation on convective heat transfer and flow features of nanofluids. ASME J. Heat Transfer 125: 151–155.
7. Brinkman HC (1952) The viscosity of concentrated suspensions and solutions. J. Chem. Phys. 20: 571–581.
8. Xuan Y, Li Q (1999) Report of Nanjing University of Sciences and Technology (in Chinese).
9. Tiwari RK, Das MK (2007) Heat transfer augmentation in a two-sided lid-driven differentially heated square cavity utilizing nanofluids. Int. J. Heat Mass Transf. 50: 2002–2018.
10. Sheikholeslami M, Gorji-Bandpy M, Ganji DD, Soleimani S (2014) Heat flux boundary condition for nanofluid filled enclosure in presence of magnetic field. J. Mol. Liq. 193: 174–184.
11. Sheikholeslami M, Hatmi M, Ganji DD (2013) Analytical investigation of MHD nanofluid flow in a semi-porous channel. Powder Technol. 246: 327–336.
12. Turkyilmazoglu M (2012) Exact analytical solutions for heat and mass transfer of MHD slip flow in nanofluids. Chem. Eng. Sci. 84: 182–187.
13. Turkyilmazoglu M (2013) Unsteady convection flow of some nanofluids past a moving vertical flat plate with heat transfer. ASME J. Heat Transfer 136: 031704.
14. Shapiro AH, Jaffrin MY, Wienberg S (1969) Peristaltic pumping with long wavelengths at low Reynolds number. J. Fluid Mech. 37: 799–825.
15. Mekheimer KhS, Husseny SZA, Abdellateef AI (2011) Effect of lateral walls on peristaltic flow through an asymmetric rectangular duct. Applied Bionics and Biomechanics 8: 1–14.
16. Abd elmaboud Y, Mekheimer KhS (2011) Non-linear peristaltic transport of a second-order fluid through a porous medium. Appl. Math. Model. 35: 2695–2710.
17. Hayat T, Abbasi FM, Hendi AA (2011) Heat transfer analysis for peristaltic mechanism in variable viscosity fluid. Chin. Phys. Lett. 28: 044701.
18. Abd elmaboud Y, Mekheimer KhS, Abdellateef AI (2013) Thermal properties of couple-stress fluid flow in an asymmetric channel with peristalsis. ASME J Heat Transfer 135: 044502.
19. Abbasi FM, Hayat T, Alsaedi A, Ahmed B (2014) Soret and Dufour effects on peristaltic transport of MHD fluid with variable viscosity. Appl. Math. Inf. Sci., 8: 211–219.
20. Hayat T, Abbasi FM, Alsaedi A, Alsaadi F (2014) Hall and Ohmic heating effects on the peristaltic transport of Carreau-Yasuda fluid in an asymmetric channel. Z. Naturforsch. 69a 43–51.
21. Abbasi FM, Hayat T, Ahmad B (2014) Peristaltic flow in an asymmetric channel with convective boundary conditions and Joule heating. J. Cent. South Univ. 21: 1411–1416.
22. Hayat T, Abbasi FM, Alhuthali MS, Ahmad B, Chen GQ (2014) Soret and Dufour effects on peristaltic transport of a third order fluid. Heat transfer Research 45: 589–603.
23. Yildirim Y, Sezer SA (2010) Effects of partial slip on the peristaltic flow of a MHD Newtonian fluid in an asymmetric channel. Math. Comput. Model. 52: 618–627.
24. Hayat T, Abbasi FM, Alsaedi A (2014) Soret and Dufour effects on peristaltic flow in an asymmetric channel. Arab. J. Sci. Eng., 39: 4341–4349.
25. Hayat T, Abbasi FM, Ahmad B, Alsaedi A (2014) Peristaltic transport of Carreau-Yasuda fluid in a curved channel with slip effects. PLoS ONE 9 (4): e95070.

26. Mustafa M, Hina S, Hayat T, Alsaedi A (2012) Slip effects on the peristaltic motion of nanofluid in a channel with wall properties. ASME J. Heat Transfer 135: 041701–041708.
27. Hayat T, Abbasi FM, Al-Yami M, Monaquel S (2014) Slip and Joule heating effects in mixed convection peristaltic transport of nanofluid with Soret and Dufour effects. J. Mol. Liq. 194: 93–99.
28. Ali N, Hussain Q, Hayat T, Asghar S (2008) Slip effects on the peristaltic transport of MHD fluid with variable viscosity. Physics Letters A. 372: 1477–1489.